Comparison of Rheological Properties of Carbon Nanotube/Polycarbonate and Carbon Black/Polycarbonate Composites

Michael D. Via,[1] Faith A. Morrison,[1] Julia A. King,[1] Jeffrey A. Caspary,[1] Owen P. Mills,[2] Gregg R. Bogucki[3]

[1]*Department of Chemical Engineering, Michigan Technological University, Houghton, Michigan 49931-1295*
[2]*Applied Chemical and Morphological Analysis Laboratory, Michigan Technological University, Houghton, Michigan 49931-1295*
[3]*Boeing Research & Technology, The Boeing Company, St. Louis, Missouri 63166-0516*

Received 9 July 2010; accepted 9 November 2010
DOI 10.1002/app.33722
Published online 25 February 2011 in Wiley Online Library (wileyonlinelibrary.com).

ABSTRACT: Conductive fillers are often added to insulating polymers to increase the composite conductivity. Adding fillers often increases the viscosity, which can make the material more difficult to process. In this study, 2–8 wt % multiwalled carbon nanotubes or 2–8 wt % carbon black were added to polycarbonate. The effects on composites' viscosities were studied with small-amplitude oscillatory shear and capillary rheometer testing. The addition of carbon nanotubes and carbon black created yield-stress materials with the yield-stresses increasing with increased filler loadings. The addition of carbon black increased the steady-shear viscosity of the composite at all shear rates for all loadings. The addition of the carbon nanotubes reduced the steady-shear viscosity of the composite at high shear rates for all loadings. This is thought to be due to an internal lubrication of the flow (enhanced disentanglement) due to the presence of the carbon nanotubes. The lubrication effect saturates once 3 wt % carbon nanotubes has been reached. The observed rheological behavior of the carbon nanotube composites is markedly different than usually seen in filled systems. A yield-stress-modified Carreau-Yasuda model was used to interpret the effects of carbon nanotube and carbon black fillers on carbon nanotube/polycarbonate and carbon black/polycarbonate composite viscosity. J Appl Polym Sci 121: 1040–1051, 2011

Key words: rheology; carbon nanotube; carbon black; polycarbonates

INTRODUCTION

Most polymer resins are electrically insulating. Increasing the electrical conductivity (1/electrical resistivity, ER) of these resins allows them to be used in other applications, such as electrostatic dissipative (ESD, e.g., handling trays used in electronic equipment assembly, etc., ER typically 10^{10} to 10^{3} ohm-cm) and moderately electrically conductive (e.g., fuel gauges, etc., ER typically 10^{2} to 10^{1} ohm-cm) applications. One approach to improving the electrical conductivity of a polymer is through the addition of a conductive filler material, such as carbon and metal.[1–14] Recently, carbon nanotubes have been used to increase the electrical conductivity of a resin.[15–26] Carbon nanotubes have many unique characteristics. For example, only a small amount of carbon nanotubes need to be added to a polymer to increase the composite's electrical conductivity without sacrificing the materials' mechanical properties and without significantly increasing the melt viscosity.[27,28] Carbon black has also been used to increase the electrical conductivity of a resin; however, it has been known to significantly increase melt viscosity at high concentrations.[12,29–31]

In this work, researchers performed compounding runs and then conducted rheological tests on carbon nanotube/polycarbonate and carbon black/polycarbonate composites. Composites containing varying amounts of a single filler (either 2–8 wt % carbon nanotubes or 2–8 wt % carbon black) were extruded and tested for rheological properties. The goal of this project was to determine and compare the effects of the carbon nanotubes and carbon black on the composite rheology. This information is needed to develop composites for ESD and semiconductive applications that can be easily fabricated.

MATERIALS AND EXPERIMENTAL METHODS

Materials

The matrix used for this project was Sabic Innovative Plastics (Pittsfield, MA) Lexan HF1130-111 polycarbonate resin. The properties of this polymer are shown in Table I.[32,33]

Correspondence to: J. A. King (jaking@mtu.edu).

TABLE I
Properties of Sabic's Polycarbonate Lexan HF 1130[32,33]

Melt flow rate (300°C/1.2 kg)	25 g/10 min
Density	1.2 g/cm^3
Number average molecular weight	46,400 g gmol^{-1}
Weight average molecular weight	82,300 g gmol^{-1}
Electrical resistivity	1×10^{17} ohm-cm
Thermal conductivity	0.19 W m^{-1} K^{-1}

Hyperion Catalysis International's (Cambridge, MA) FIBRIL^{TM} nanotubes were used in this study. This is a conductive, vapor grown, multi-walled carbon nanotube (CNT). They are produced from high purity, low molecular weight hydrocarbons in a proprietary, continuous, gas phase, catalyzed reaction. The outside diameter of the tube is 10 nm and the length is 10 μm, which gives an aspect ratio (length/diameter) of 1000. Because of this high aspect ratio, very low concentrations of nanotubes are needed to produce an electrically conductive composite. This material was provided by Hyperion Catalysis International in a 15 wt % FIBRIL^{TM} masterbatch MB6015-00 in polycarbonate. Table II shows the properties of this carbon nanotube.[18,22,34]

Ketjenblack EC-600 JD is an electrically conductive carbon black available from Akzo Nobel (Chicago, IL). The highly branched, high surface area carbon black structure allows it to contact a large amount of polymer, which results in improved electrical conductivity at low carbon black concentrations (often 5–7 wt %). The properties of Ketjenblack EC-600 JD are given in Table III.[35] The carbon black is sold in the form of pellets that are 100 μm to 2 mm in size and, upon mixing into a polymer, easily separates into primary aggregates 30 to 100 nm long.[35] Figure 1 shows a diagram of the carbon black structure.

The concentrations (shown in wt % with the corresponding vol. % calculated using 1.75 g cm^{-3} for the carbon nanotube density) for all of the single-filler composites tested in this research are shown in Table IV.[18,22] Table V shows the concentrations used for the carbon black/polycarbonate composites. In this and following tables, figures, and text, the abbreviation "PC" is used to signify polycarbonate,

TABLE II
Properties of FIBRIL^{TM} Carbon Nanotubes[18,22,34]

Composition	Carbon
Diameter	0.01 μm
Length	10 μm
Morphology	Graphitic sheets wrapped around a hollow 0.005 μm core
BET (N_2) surface area	250 m^2 g^{-1}
Density	2.0 g cm^{-3} for the nanotube wall; 1.75 g cm^{-3} for the hollow nanotube

TABLE III
Properties of Akzo Nobel Ketjenblack EC-600 JD Carbon Black[35]

Electrical resistivity	0.01–0.1 Ohm-cm
Aggregate size	30–100 nm
Specific gravity	1.8 g cm^{-3}
Apparent bulk Density	100–120 kg m^{-3}
Ash content, max	0.1 wt %
Moisture, max	0.5 wt %
BET surface area	1250 m^2 g^{-1}
Pore volume	480–510 cm^3/100 g

"CNT" is used for carbon nanotube (FIBRIL^{TM}), and "CB" is used for carbon black (Ketjenblack EC-600 JD). Tables IV and V also show the rheology and ER results that will be described later in this article.

Test specimen fabrication

Prior to extrusion and injection molding, the Lexan HF1130-111 polycarbonate pellets were dried in an indirect heated dehumidifying drying oven at 121°C for 12 h. The Hyperion fibrils MB6015-00 were dried in an indirect heated dehumidifying drying oven at 121°C for 6 h. Ketjenblack EC-600 JD carbon black was used as received. The extruder used was an American Leistritz Extruder Corp. (Somerville, NJ) Model ZSE 27. This extruder has a 27 mm corotating intermeshing twin screw with 10 zones and a length/diameter ratio of 40. The pure polycarbonate pellets and the Hyperion FIBRIL^{TM} masterbatch MB6015-00 (containing 15 wt % carbon nanotubes) pellets were premixed in a V cone blender and then introduced in Zone 1. The screw design, which is shown in Figure 2, was chosen to obtain a minimum amount of filler degradation, while still dispersing the filler well in the polymer. For the CB/PC composites, Figure 3 shows the screw design used. The pure polycarbonate pellets were introduced in Zone 1. Ketjenblack EC-600 JD was introduced in Zone 5. Again, this screw design was chosen to obtain a minimum amount of filler degradation, while still dispersing the fillers well in the polymers.

After passing through the extruder, the polymer strands (3 mm in diameter) entered a water bath and subsequently a pelletizer that produced nominally 3-mm long pellets. After extrusion, the polycarbonate-based composites were dried in an indirect-heated

Figure 1 Carbon black diagram.

TABLE IV
Composite Properties: Electrical Resistivity Showing Percolation Below 2 wt %; Yield Stress from the Small Amplitude Oscillatory Shear (SAOS) Data; Yield Stress, Matrix-Zero-Shear-Viscosity and Infinite-Shear Viscosity Parameters Used in Modeling Discussed in Text

Formulation	Filler (wt %)	Filler (vol %)	Electrical resistivity (Ω-cm)	Yield stress from SAOS (Pa)	Yield stress in CY model (Pa)	η_0 (Pa s)
PC	0.0	0.0	$1.06 \times 10^{17} \pm 7.96 \times 10^{16}$; $n = 7$	0	0	700
2CNT	2.0	1.38	4605 ± 1115; $n = 6$	2500	3500	450
3CNT	3.0	2.08	216 ± 44; $n = 6$	17,000	5000	380
4CNT	4.0	2.78	73 ± 10; $n = 6$	43,000	7000	380
5CNT	5.0	3.48	43 ± 7; $n = 6$	75,000	9000	380
6CNT	6.0	4.19	18 ± 2; $n = 6$	87,000	12,000	380
8CNT	8.0	5.63	7.8 ± 0.4; $n = 6$	220,000	20,000	380

The parameters in the last three columns were used to fit steady shear data to the function given in eq. (12). For all fits $\lambda = 0.003$, $a = 1$, and $n = 0.5$. Different yield stresses were obtained in SAOS and steady shear since the Cox-Merz rule was not observed to hold.

dehumidifying drying oven at 121°C for 12 h and then stored in moisture barrier bags.

A Niigata (Tokyo, Japan) injection-molding machine, model NE85UA$_4$, was used to produce test specimens. This machine has a 40 mm diameter single screw with a length/diameter ratio of 18. The lengths of the feed, compression, and metering sections of the single screw are 396, 180, and 144 mm, respectively. A four-cavity mold was used to produce 3-mm thick, 6.4 cm diameter disks (end gated), 3.1 mm thick by 127 mm long by 12.7 mm wide flexural bars (end gated), and 3.3 mm thick ASTM Type I tensile bars (end gated).

Field emission scanning electron microscope (FESEM) and transmission electron microscopy (TEM) test methods

To view the CNT in the CNT/PC composite, a Hitachi *S*-4700 (Pleasanton, CA) Cold Field Emission Scanning Electron Microscope (FESEM) was used to view the cryrofractured surface of the CNT/PC composite. The samples were prepared for observation by cryo-fracture where the composite was submerged in liquid nitrogen until frozen then quickly retracted and fractured. Afterward, the samples were attached to aluminum mounting discs and were observed in the FESEM at 2 kV accelerating voltage, 2 mm working distance, using the upper secondary electron detector. This method was used to view the CNT.

To view the dispersion of the CNT in polycarbonate, the following method was used. Ultra-thin ($\sim$ 50 nm) TEM sections of the composite were prepared by Leica UCT ultramicrotome (Bannockburn, IL). The sections were supported on a copper 300 mesh lacey formvar carbon-coated grid and then examined using a JEOL JEM-4000FX operated at 200 kV accelerating voltage. The CNT distributions were imaged at a magnification of 12000×, and digital images were acquired using a Gatan Orius (Pleasanton, CA) camera. This technique was used to view the dispersion of the CNT in polycarbonate.

To view the CB in the CB/PC composite, the following method was used. A JEOL JSM-7500F (Tokyo, Japan) Field Emission Scanning Electron

TABLE V
Composite Properties: Electrical Resistivity Showing Percolation Between 3 and 4 wt %; Yield Stress from the SAOS Data; Yield Stress, Matrix-Zero-Shear-Viscosity and Infinite-Shear Viscosity Parameters Used in Modeling Discussed in Text

Formulation	Filler (wt %)	Filler (vol %)	Electrical resistivity (ohm-cm)	Yield stress from SAOS (Pa)	Yield stress in CY model (Pa)	η_0 (Pa s)	a	λ
PC	0	0.0	$1.26 \times 10^{17} \pm 3.35 \times 10^{16}$; $n = 6$	0	0	700	0.7	0.0006
2CB	2	1.34	$4.05 \times 10^{16} \pm 2.66 \times 10^{16}$; $n = 6$	1200	1200	850	1	0.0008
3CB	3	2.01	$2.85 \times 10^{15} \pm 4.58 \times 10^{14}$; $n = 6$	5000	4000	950	1	0.0008
4CB	4	2.69	$1.17 \times 10^{5} \pm 7.77 \times 10^{4}$; $n = 8$	11,000	6000	1100	1	0.001
5CB	5	3.38	2474 ± 646.2; $n = 8$	21,000	9000	1300	1	0.001
6CB	6	4.07	649.2 ± 17.6; $n = 8$	37,000	12,000	1400	1	0.001
8CB	8	5.46	122.2 ± 4.0; $n = 8$	120,000	29,000	2000	0.7	0.001

The parameters in the last three columns were used to fit steady shear data to the function given in eq. (12). For all fits $n = 0$. Different yield stresses were obtained in SAOS and steady shear since the Cox-Merz rule was not observed to hold.

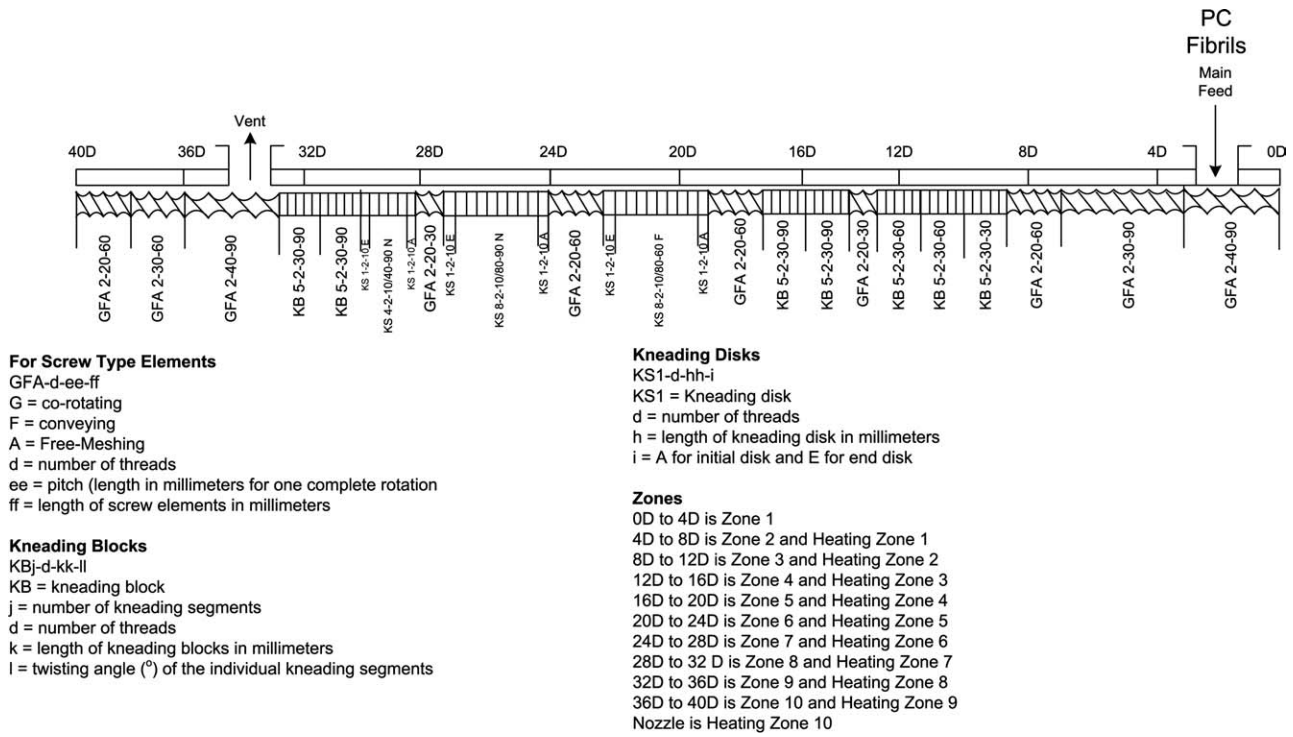

Figure 2 CNT/PC extruder screw design.

Microscope (FESEM) was used to view the surface of the CB/PC composite (3.1-mm thick by 12.7-mm wide cross section from an injection flexural bar). The sample was prepared for observation by mounting the composite in a cast epoxy puck. Then the surface was polished with SiC to a no. 4000 grit finish, followed by polishing with a 1 μm alumina/water slurry on a rotating lap cloth, and then finally with a 0.05 μm alumina/water slurry in a Buehler Vibromet (Lake Bluff, IL) polisher for 2 h. The composite surface was then

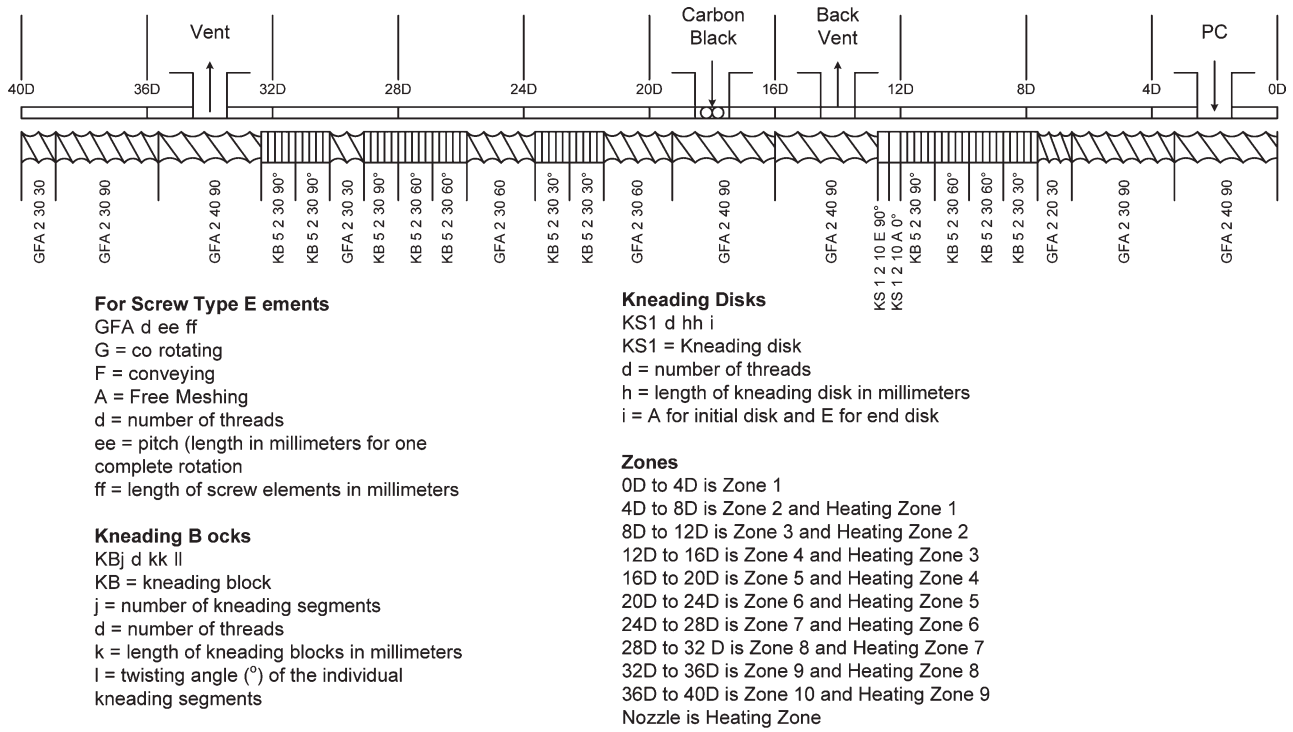

Figure 3 CB/PC extruder screw design.

etched in O_2 plasma at 23°C and 0.28 Torr for 1 h and then sputter coated with ~ 10 nm layer of gold. Finally, the samples were observed in the FESEM at 10 kV accelerating voltage, 6 mm working distance using the upper secondary electron detector. These samples were prepared and photomicrographs taken by Huang Wu at the Composite Materials and Structures Center at Michigan State University.

Small amplitude oscillatory shear test method

Small-amplitude oscillatory shear (SAOS) complex viscosity measurements were taken using a Bohlin C-VOR rheometer (Malvern Instruments; Wesborough, MA) with 25 mm diameter parallel plates and a 3-mm gap according to ISO 6721-10.[36] Samples for parallel-plate testing were prepared by cutting the polycarbonate-based injection-molded 6.4 cm diameter disks into two 2.5-cm diameter disks. Five total 2.5 cm diameter disks were selected for parallel-plate rheometry for each formulation. The 2.5 cm diameter disks were vacuum dried for 6 h at 100°C and 30-in. Hg vacuum and subsequently for another 6 h at 120°C and 27-in. Hg vacuum. For the CNT/PC composites, SAOS tests were run at 210, 230, 250, 270, 290, 310, 330, and 350°C beginning with an amplitude sweep varying from 0.1 to 10% strain to determine the extent of the linear-viscoelastic regime. For the CB/PC composites, SAOS tests were run over a more limited temperature range of 250, 270, 290, 310, and 330°C (determined to be the most effective from analyzing the CNT/PC results) beginning with an amplitude sweep varying from 0.1 to 10% strain to determine the extent of the linear-viscoelastic regime. Frequency sweeps from 0.1 to 100 rad s^{-1} at an amplitude of 1.0% were taken in a "ramp-up then ramp-down" fashion.

The linear-viscoelastic elastic modulus $G'(\omega)$ and viscous modulus $G''(\omega)$ were time-temperature shifted to produce master curves of the elastic modulus G_r' $(a_T\omega)$ and loss modulus $G_r''(a_T\omega)$ versus $a_T\omega$ at 270°C.

$$G_r'(a_T\omega) \equiv \frac{G'(T)T_{\text{ref}}\rho_{\text{ref}}}{T\rho}$$

$$G_r''(a_T\omega) \equiv \frac{G''(T)T_{\text{ref}}\rho_{\text{ref}}}{T\rho} \quad (1)$$

where ω is the oscillation frequency in radians s^{-1}, $a_T\omega$ is the shift factor, T_{ref} (270°C) is the reference temperature for the superpositioning, ρ_{ref} is the density of the material at the reference temperature, T is the test temperature, and ρ is the sample density at the test temperature.[37] The shift factors were obtained such that the shifted data best-fit a single master curve at the reference temperature. Complex viscosities, $\eta^*(\omega)$, were calculated from G' and G'' as

$$\eta^*(\omega) \equiv \frac{\sqrt{G'^2(\omega) + G''^2(\omega)}}{\omega} \quad (2)$$

For many linear polymers, the complex viscosity function $\eta^*(\omega)$ obtained in small-amplitude oscillatory shear has the same shape as the steady-shear viscosity function $\eta(\dot{\gamma})$ when compared at $\omega = \dot{\gamma}$. This is known as the Cox-Merz rule.[37,38] In this work we tested the validity of the Cox-Merz rule for CNT/PC and CB/PC composites.

Although the Bohlin C-VOR rheometer is capable of steady shear, sample stiffness prevents us from measuring $\eta(\dot{\gamma})$ at the shear rates that interest us. Thus, for steady shear measurements, we used a capillary rheometer.

Capillary rheometer test method

Steady-shear rheometry was performed on the extruded pellets and neat polycarbonate pellets on a Goettfert Rheotester 1000 (Rock Hill, SC). All the pellets were dried in an indirect heated dehumidifying oven at 121°C for 12 h and then further dried in a vacuum oven for 6 h at 100°C and 30 in. of Hg. The materials (polycarbonate and 2, 3, 4, 5, 6, and 8 wt % CNT in polycarbonate) were tested at 270, 300, and 320°C. The sample of neat polycarbonate could not be tested at 320°C due to thermal degradation of the polymer. The CB/PC composites were tested at 270 and 300°C. The tests were performed using a 30-mm long by 1-mm diameter capillary and with a 20-mm long by 1-mm diameter capillary. Steady-state pressure drops as a function of flow rate were recorded. The test method used was ASTM D3835.[39]

True steady shear viscosity was calculated from capillary flow raw data as follows. The apparent shear rate in the capillary flow, $\dot{\gamma}_a$, was calculated from flow rate Q using eq. (3),

$$\dot{\gamma}_a = \frac{4Q}{\pi R^3} \quad (3)$$

where Q is the volumetric flow rate (in units of mm^3 s^{-1}), and R is the radius (in units of mm) of the capillary.[37] For capillary flow, the shear stress at the wall τ_R (in units of Pa) is given by:

$$\tau_R = \frac{R\Delta P}{2L} \quad (4)$$

where ΔP is the pressure drop over the capillary of radius R and length L. For non-Newtonian fluids, the relationship between the true shear rate at the wall of the capillary $\dot{\gamma}_R$ and the apparent shear rate $\dot{\gamma}_a$ (what the shear rate would be for a Newtonian fluid) is given by the following equation.[37]

$$\dot{\gamma}_R = \dot{\gamma}_a \left[\frac{1}{4} \left(3 + \frac{d \ln \dot{\gamma}_a}{d \ln \tau_R} \right) \right] \quad (5)$$

Equation 5 is valid for any fluid. The quantity in square brackets is called the Weissenberg-Rabinowitsch correction. For Newtonian fluids, the correction factor is one and $\dot{\gamma}_R = \dot{\gamma}_a$.

For our experiments, the apparent shear rate $\dot{\gamma}_a$ was varied (50, 100, 200, 500, 1000, and 2000 s^{-1}), and the pressure near the entrance to the capillary was measured using a pressure transducer. Based on eq. (4), the shear stress at the wall τ_R was calculated. A quadratic equation was fit for the $\ln(\dot{\gamma}_a)$ versus $\ln(\tau_R)$ data ($R^2 > 0.99$). After the derivative in eq. (5) was calculated, the shear rate at the capillary wall $\dot{\gamma}_R$ was determined. Finally, the steady shear viscosity η (in units of Pa s) was calculated from eq. (6).[37]

$$\eta = \frac{\tau_R}{\dot{\gamma}_R} \quad (6)$$

The data of viscosity versus shear rate were time–temperature superposed to produce master curves of steady shear viscosity, η_r, versus $a_T\dot{\gamma}$ at 270°C in a similar manner to that used to superposition the SAOS data previously using

$$\eta_r(a_T\dot{\gamma}) \equiv \frac{\eta(T)T_{\text{ref}}\rho_{\text{ref}}}{a_T T \rho} \quad (7)$$

where $\dot{\gamma}$ is the shear rate in 1/s, and a_T is the shift factor.[37]

The final results of the viscosity η as a function of the shear rate $\dot{\gamma}$ are reported, as per the usual practice, as log η versus log $\dot{\gamma}$ (time–temperature superposed). The function a_T (T) is also reported giving complete access to all the data. A horizontal line is indicative of a Newtonian fluid, where η is constant. If the viscosity decreases as the shear rate is increased, the fluid is called shear-thinning. Many polymers, including our polycarbonate, exhibit shear-thinning behavior.

Electrical resistivity (ER) test method

Since the rheology results discussed in this article are compared with the electrical percolation threshold, these ER test methods are described here. For samples with an electrical resistivity $>10^6$ ohm-cm, the volumetric electrical conductivity test was conducted. In this method, a constant voltage (100 V) was applied to the as-molded test specimen, and the resistivity was measured according to ASTM D257 using a Keithley (Cleveland, OH) 6517A Electrometer/High Resistance Meter and an 8009 Resistivity Test Fixture.[40] The Keithley 6524 High Resistance Measurement Software was used to automate the conductivity measurement. Each test specimen was an injection molded disk that was 6.4 cm in diameter and 3.4-mm thick. At least six samples were tested for each formulation. Prior to testing, the samples were conditioned at 23°C and 50% relative humidity for 2 days.

The in-plane volumetric electrical resistivity of the center 60-mm long, 3.3-mm thick, 12.7-mm wide tensile bars (rectangular necked area) injection molded tensile bars was determined according to ASTM D 4496 at 23°C for samples with an electrical resistivity $<10^6$ ohm-cm.[41] Prior to testing, the samples were conditioned at 23°C and 50% relative humidity for 2 days. At least six samples were tested for each formulation. This test was conducted with two probes. In the two probe method, the tensile bar was scratched with a razor blade, placed in liquid nitrogen, and then broken manually at the desired location. Hence, a fracture surface was created on both ends of the in-plane sample. Then the 3.3-mm thick by 12.7-mm wide ends were coated with silver paint and allowed to dry for 1 h. One probe was placed on each silver painted fracture surface and a constant voltage was placed across the sample using a Keithley 2400 Source Meter. The resulting current was also measured on this same Keithley 2400 and the ER was calculated according to ASTM D 4496.

RESULTS

Field emission scanning electron microscope (FESEM) and transmission electron microscope (TEM) results

Figure 4 shows the CNT (white tubes) in the sample containing 6 wt % CNT in polycarbonate. Figure 5 shows good dispersion of the CNT in 2 and 8 wt % CNT composites. Conductive networks of CNT are seen in the 6 and 8 wt % CNT samples. Figure 6 shows the CB (white spheres) in the sample containing 6 wt % CB. As expected, a nanosize highly structured carbon black is seen with numerous conductive paths present due to the close proximity of the carbon black to each other.[12] Huang Wu took this photomicrograph at the Composite Materials and Structures Center at Michigan State University.

Small-amplitude oscillator shear (SAOS) results

The SAOS master curves for all the CNT/PC composites are shown in Figure 7, with the corresponding shift factors given in Figure 8. The SAOS master curves for all the CB/PC composites are shown in Figure 9, with the corresponding shift factors given in Figure 10. In Figures 7 and 9, the plots of log η^* as a function of log frequency show a slope of -1 at low frequency. This behavior that is consistent with the presence of a yield stress as we now discuss.

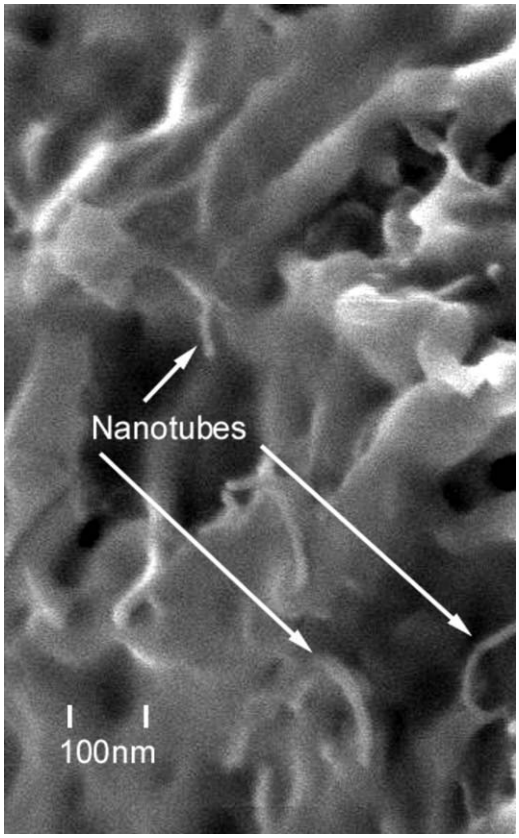

Figure 4 Field emission scanning electron microscope photomicrograph of 6 wt % carbon nanotubes in polycarbonate.

For constant-viscosity fluid that has a yield stress (a Bingham plastic), the shear stress is given by

$$\tau_{21} = \mu_0\dot{\gamma} + \tau_0 \tag{8}$$

where τ_{21} is the shear stress, $\dot{\gamma}$ is the shear rate, μ_0 is the viscosity parameter of the model, and τ_0 is the yield stress.[37] Since viscosity η is defined as the ratio

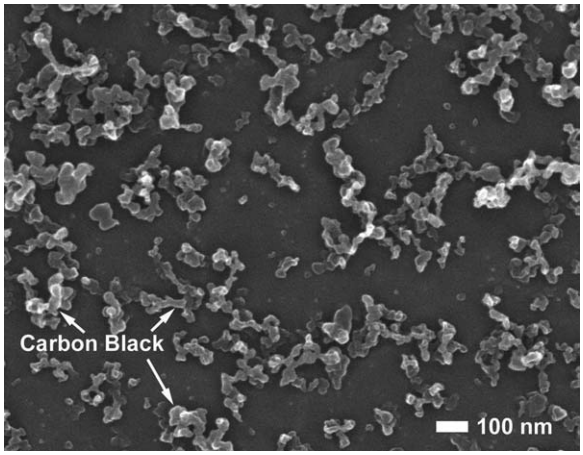

Figure 6 Field emission scanning electron microscope photomicrograph of 6 wt % carbon black in polycarbonate.

of the shear stress to the shear rate, $\eta \equiv \tau_{21}/\dot{\gamma}$, we see that for the Bingham model

$$\eta = \mu_0 + \frac{\tau_0}{\dot{\gamma}} \tag{9}$$

on a log-log graph eq. (9) at low values of shear rate $\dot{\gamma}$ yields a line of slope -1, as shown in eqs. (10) and (11).

$$\log\eta = \log\left(\mu_0 + \frac{\tau_0}{\dot{\gamma}}\right) \tag{10}$$

$$\lim_{\dot{\gamma}\to 0}\left[\log\left(\mu_0 + \frac{\tau_0}{\dot{\gamma}}\right)\right] = \log\tau_0 - \log\dot{\gamma} \tag{11}$$

We can estimate the yield stress in a system by noting the value of the viscosity at $\dot{\gamma} = 1\ s^{-1}$, provided the data exhibit the limiting behavior at this value of shear rate. The yield stresses estimated in this way from the data in Figures 7 and 9 are given in Tables IV and V.

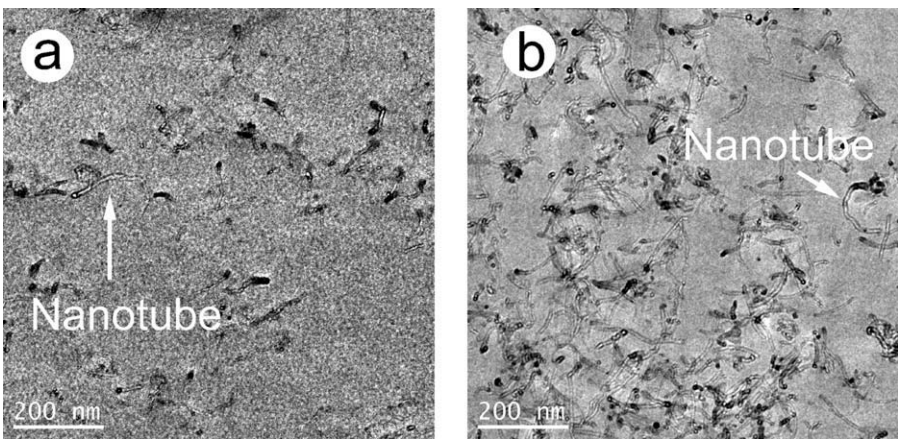

Figure 5 TEM photomicrographs of carbon nanotube (CNT)/polycarbonate composites (a) 2 wt % CNT (b) 8 wt % CNT.

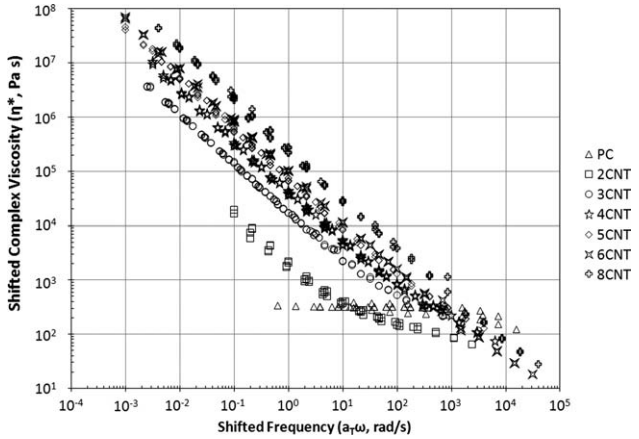

Figure 7 Time-temperature shifted complex viscosity as a function of shifted frequency for carbon nanotube/polycarbonate composites studied at 270°C.

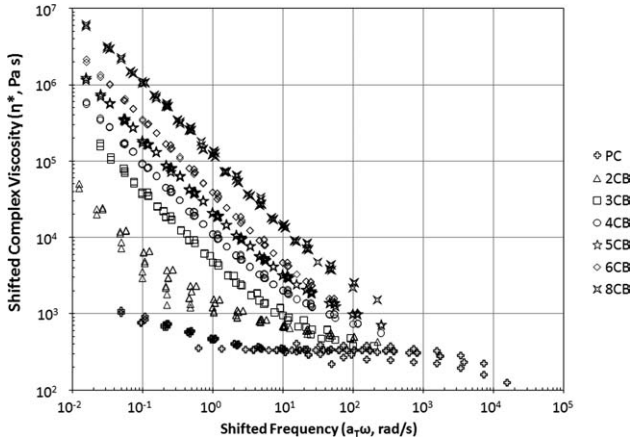

Figure 9 Time-temperature shifted complex viscosity as a function of shifted frequency for carbon black/polycarbonate composites studied at 270°C.

Capillary rheometer results: CNT/PC

The steady-shear master curves obtained from the capillary rheometer for all the CNT/PC composites are shown in Figures 11 and 12 with the corresponding shift factors a_T given in Figure 8. Also included in Figures 11 and 12 are fits to a model (CY) that will be discussed later.

In Figure 11 the pure PC (topmost curve) shows a typical flow curve, with a Newtonian plateau of approximately $\eta_0 = 700$ Pa s observed at low shear rates, and shear thinning observed at the highest shear rates. As CNT is added to the PC (0–4 wt % CNT), the viscosities of the resulting composites are observed to decrease by up to a factor of two (Fig. 11). This is unusual behavior, as most carbon/thermoplastic composites show an increase in viscosity as filler loading is increased.[27,42–46] At still higher loadings (4–8 wt % CNT in Fig. 12) and low shear rates, the viscosities rise as CNT is added to the polycarbonate. The increases in low-shear-rate viscosity are small for low filler loadings but become quite substantial at the highest loadings (see Fig. 12 for 8 wt % CNT).

The observed rheological behavior of CNT/PC composites, both in SAOS and in steady capillary flow, is quite unusual for composites, and the cause of the behavior is not immediately obvious. However, Lee et al. has recently noted similar behavior in CNT/PC composites.[47] In addition, the Cox-Merz rule is not followed in our materials.[37,38] The Cox-Merz rule states that the steady viscosity $\eta(\dot{\gamma})$ is often found to be equal to the complex viscosity $\eta^*(\omega)$ when they are compared at $\dot{\gamma} = \omega$; this was not found to be true even for pure polycarbonate at low deformation rates (for PC $\eta_0 = 700$ Pa s, $\eta_0^* = 320$ Pa s). The SAOS behavior indicates that a yield stress appears and grows with filler content (Fig. 7 and Table IV).

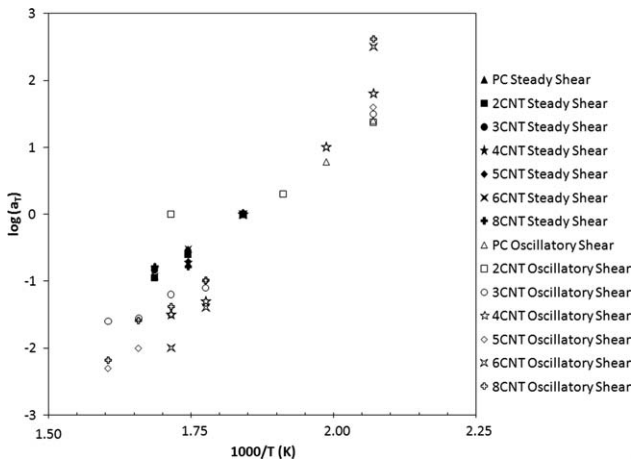

Figure 8 Time-temperature shift factors a_T for both steady and oscillatory rheological data of carbon nanotube/polycarbonate composites as a function of inverse temperature.

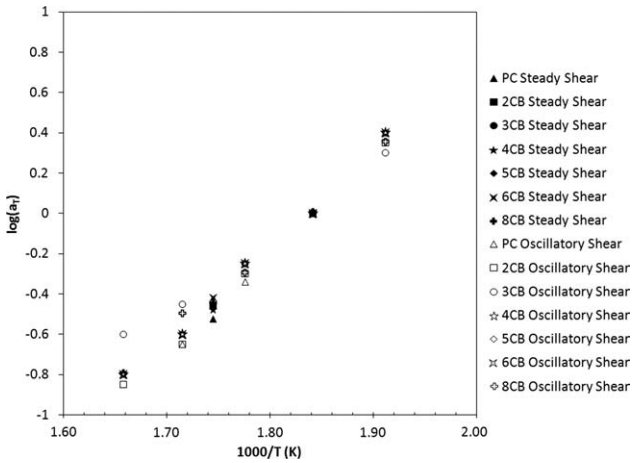

Figure 10 Time-temperature shift factors a_T for both steady and oscillatory rheological data of carbon black/polycarbonate composites as a function of inverse temperature.

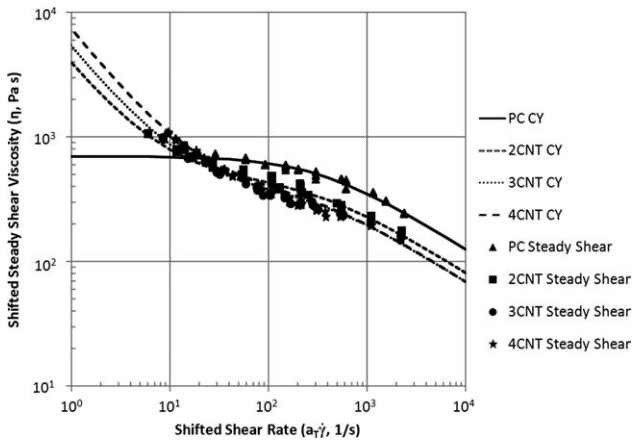

Figure 11 Time-temperature shifted steady-shear viscosity as a function of shifted shear rate for carbon nanotube/polycarbonate composites studied at 270°C. Compositions range from pure polycarbonate (0 wt % CNT) to 4 wt % CNT. Lines in the figure represent the Carreau-Yassuda (CY) model discussed in the text.

The steady shear viscosity, however, shows a complex set of behaviors (Figs. 11 and 12).

Guided by the yield-stress behavior indicated in the SAOS results, we can understand the observed steady shear capillary data of the CNT/PC composites by postulating that yield stress grows with CNT content and that this is accompanied by a decrease in the apparent zero-shear plateau (η_0) of the polycarbonate matrix. To see how these two effects would change a sample's rheological behavior, we fit a modified Carreau-Yassuda model[37,48] to our $\eta(\dot{\gamma})$ data using the parameters given in Table IV. The model we used is shown in eq. (12):

$$\eta(\dot{\gamma}) = \frac{\tau_0}{\dot{\gamma}} + \eta_0(1 + (\dot{\gamma}\lambda)^a)^{\frac{n-1}{a}} \qquad (12)$$

where τ_0 is the yield stress, η_0 is the zero shear viscosity of the matrix polymer, λ is a relaxation time (which determines when shear-thinning starts), a is an exponent parameter, and n is a power-law index. The fits are shown in Figures 11 and 12 and are labeled CY to represent the modified Carreau-Yasuda model. The parameters used in the curve fits are given in Table IV.

The rheological model given in eq. (12) has two essential parts, a yield stress and a zero-shear viscosity. The yield stress causes the model viscosity curves to exhibit a slope of -1 at low shear rates. At high shear-rates the rheological model in eq. (12) is dominated by the zero-shear behavior of the matrix, and the predicted viscosity curve shear thins with a power-law index of 0.5. In between these two limits, there is crossover behavior that, for the parameters we have used, mimics the behavior of the CNT/PC systems studied here.

The values of the parameters used in our fits can give us an idea of what may be happening within the CNT/PC composites. The yield-stress parameters that were used in the steady shear fits imply that the data show a yield stress, a conclusion that is corroborated by the SAOS data discussed earlier. The yield-stress parameters used in the steady shear fit are not the same as those measured in SAOS, they are off by up to a factor of ten, but the trend with CNT composition is similar. No correspondence between the two estimates of yield stress (SAOS and fits to steady-shear viscosity) is expected given that the Cox-Merz rule is not followed in our composites. The matrix-zero-shear-viscosity parameters used in the fits indicate that η_0 decreases with increasing weight fractions up to 3 wt % (from 700 to 380 Pa s) and then saturates at that low level (380 Pa s) as the wt % CNT rises to 8 wt % (Table IV). The parameters $\lambda = 0.003$ and $n = 0.5$ were not varied in these fits.

The growth in yield stress implied by the steady-shear fits (from 3.5 to 20 kPa) is consistent with the building of a network among carbon nanotubes throughout the composite. The electrical percolation threshold for this composite is below 2 wt % (Table IV shows mean, standard deviation, and number of samples tested), which corroborates the existence of a stress-bearing network for these composites, even at low loadings.[28] The steady-shear modeling results and the SAOS results both indicate that yield stress grows continuously with filler loading.

The model's suggested variation of the matrix-zero-shear-viscosity parameter η_0 may be interpreted as a high-shear-rate lubrication process occurring as a result of the presence of the carbon nanotubes. The

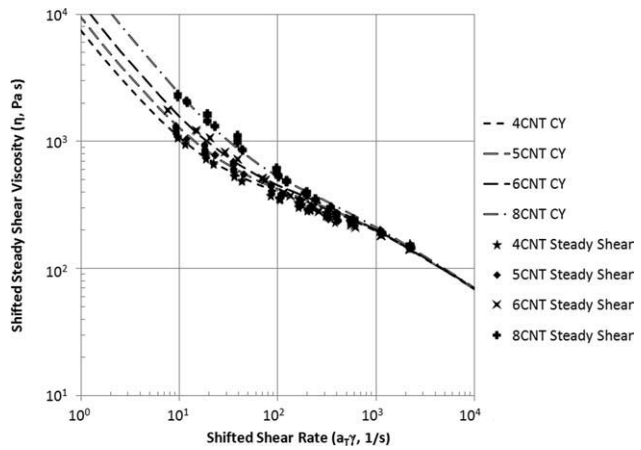

Figure 12 Time-temperature shifted steady-shear viscosity as a function of shifted shear rate for carbon nanotube/polycarbonate composites studied at 270°C. Compositions range from 4 wt % CNT to 8 wt % CNT. Lines in the figure represent the Carreau-Yassuda (CY) model discussed in the text.

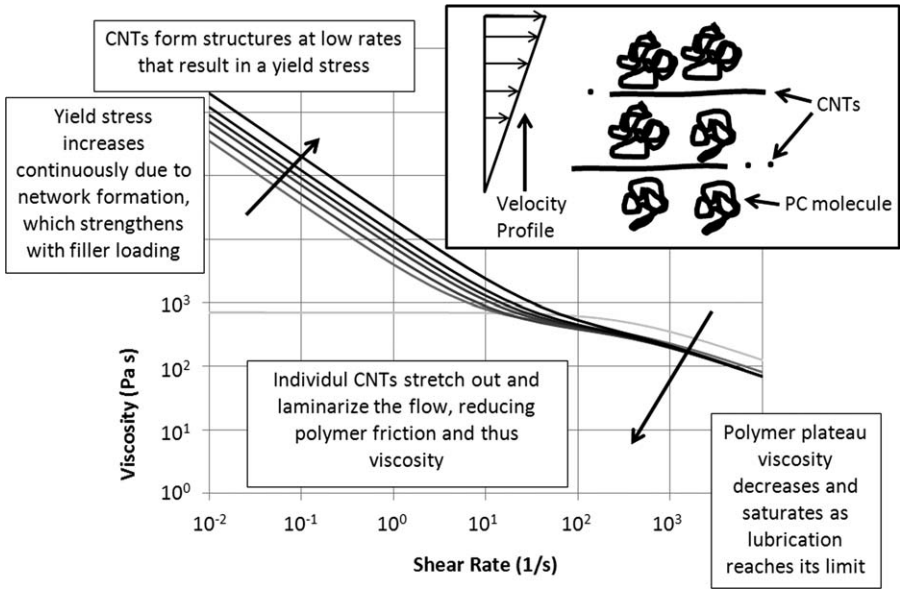

Figure 13 Schematic of a possible mechanism for the lubrication observed at high shear rates. The entangled polycarbonate molecules are somewhat straightened out and forced into layers in such a way that the layers of fluid can flow with less friction than if the CNT clusters were not present.

high-shear-rate data in the viscosity curve reflects the entangled flow of the polycarbonate. In this flow regime, the pure polycarbonate is shear-thinning, indicating that the individual molecules are disentangling during the flow of the pure polycarbonate. For the composites studied here, our modeling suggests that the presence of the nanotubes may cause an enhancement of disentanglement at high shear rate $\dot{\gamma}$. We visualize that the carbon nanotubes cause a kind of layering or laminarization of the flow. This effect is postulated to be caused by the presence of extended carbon nanotubes or nanotube clusters and log-rolling carbon nanotubes or nanotube clusters (Fig. 13). The carbon nanotubes allow greater relative motion among the layers of entangled polymers, allowing a reduction of overall friction in the flow. This reduction would be reflected in a reduced η_0. It is reasonable that this type of lubrication effect would saturate at some level, and saturation of η_0 at a value of 380 Pa s is observed in our fits. The situation we envision for the CNT composites is somewhat reminiscent to the events that are thought to occur in turbulent flow drag reduction.[48] In turbulent drag reduction, the stretching out of polymers in dilute solution is thought to somewhat straighten out the turbulent flow, allowing the net amount of friction to be reduced.

Capillary rheometer results and discussion: CB/PC

The steady-shear master curves obtained from the capillary rheometer for all the CB/PC composites are shown in Figures 14 and 15 with the corresponding shift factors a_T given in Figure 10. Also included in Figures 14 and 15 are fits to the model (CY) that has been previously discussed.

In Figures 14 and 15, as CB is added to the PC, the steady shear viscosities of the resulting composites are observed to increase from 700 to 2000 Pa s. This is the expected behavior, as most carbon/thermoplastic composites show an increase in viscosity as filler loading is increased.[27,42–46] At all shear rates, the viscosities rise as CB is added to the polycarbonate. The increases in low-shear-rate viscosity are substantial at the highest loadings (see Fig. 15 for

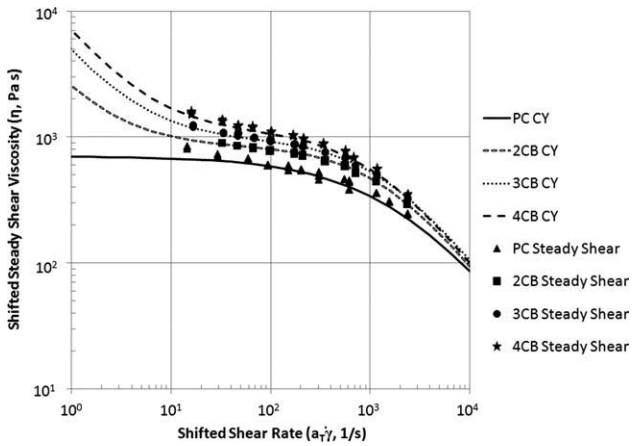

Figure 14 Time-temperature shifted steady-shear viscosity as a function of shifted shear rate for carbon black/polycarbonate composites studied at 270°C. Compositions range from pure polycarbonate (0 wt % CB) to 4 wt % CB. Lines in the figure represent the Carreau-Yassuda (CY) model discussed in the text.

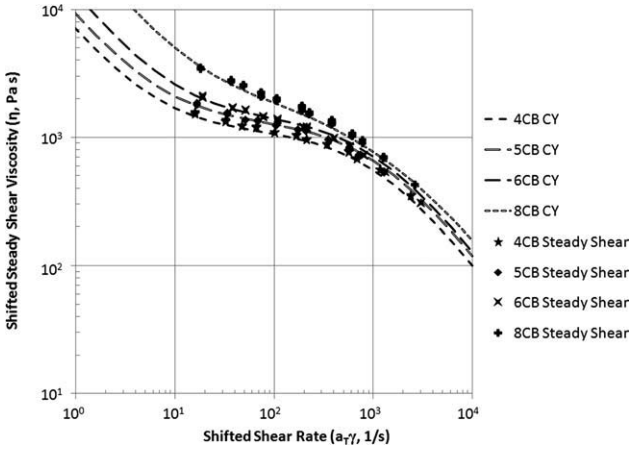

Figure 15 Time-temperature shifted steady-shear viscosity as a function of shifted shear rate for carbon black/polycarbonate composites studied at 270°C. Compositions range from 4 wt % CB to 8 wt % CB. Lines in the figure represent the Carreau-Yassuda (CY) model discussed in the text.

8 wt % CB). At high shear rates, shear thinning effects reduce the increase in viscosity (see Fig. 15) due to higher filler loadings (4–8 wt % CB). No crossover or lubrication effects were observed.

The growth in yield stress implied by the steady-shear fits (from 1.2 to 29 kPa) is consistent with the building of a network among carbon black agglomerates throughout the composite. The electrical percolation threshold for this composite is between 3 and 4 wt % CB ($\sim$ 2.3 vol % CB; Table V shows mean, standard deviation, and number of samples tested), which corroborates the existence of a stress-bearing network for these composites, even at low loadings.[49] The steady-shear modeling results and the SAOS results both indicate that yield stress grows continuously with filler loading. The parameter $n = 0$ was not varied in the CB/PC fits.

CONCLUSIONS

The object of this research was to determine the effect of the addition of various amounts of multiwalled carbon nanotube or carbon black on CNT/PC and CB/PC composite viscosities. Small-amplitude oscillatory shear measurements determined that the addition of multiwalled carbon nanotubes or carbon black to a PC matrix created yield-stress materials. The apparent yield stress from SAOS and that reflected in steady-shear modeling increased monotonically with increased filler loadings. The growth of apparent yield stress is believed to be due to the creation of a stress-bearing structure consistent with CNT and CB percolation.[28,49] Steady shear capillary rheometry measurements on all CB composites showed an increase in composite viscosity with increasing filler loading levels for all shear rates, which is a classic filler effect. Steady shear capillary rheometry measurements on all CNT composites showed a decrease in composite viscosity with increasing filler loading levels for high shear rates, which is different from classic behavior. This viscosity reduction is consistent with an internal lubrication effect caused by the carbon nanotubes or by clusters of carbon nanotubes. This effect is imagined to be due to flow laminarization caused by the presence of the carbon nanotubes stretched out in the direction of flow and/or log-rolling carbon nanotubes/nanotube clusters oriented perpendicular to the direction of flow. For composites with 3, 4, 5, 6, and 8 wt % CNT there is very little additional change in high shear rate viscosity due to the addition of filler above 2 wt % CNT, which is believed to be caused by a saturation of the laminarization effect described above. Both estimates of yield stress (SAOS and steady-shear modeling) grow as wt % CNT is added; this effect and the laminarization effect are both captured by a viscosity model based on a modified Carreau-Yassuda equation. The Cox-Merz law was not observed to hold for polycarbonate, CNT/PC composites, or CB/PC composites.

The authors thank the American Leistritz technical staff for recommending an extruder screw design. The authors also thank Timothy Jozokos (Hyperion Catalysis International, Inc.) for providing technical advice on this project. The authors thank Claire Drom and Kiersten Schierbeek for assisting with microscopy work. The authors thank Timothy Gasperich for his work extruding and injection molding these materials. The authors also thank Huang Wu at the Composite Materials and Structures Center at Michigan State University for preparing and taking FESEM photomicrographs of the CB/PC composites.

References

1. Taipalus, R.; Harmia, T.; Zhang, M. Q.; Friedrich, K. Compos Sci Tech 2001, 61, 801.
2. Agari, Y.; Uno, T. J. J Appl Polym Sci 1985, 30, 2225.
3. Bigg, D. M. Polym Eng Sci 1977, 17, 842.
4. Bigg, D. M. Adv Polym Technol 1984, 4, 255.
5. Narkis, M.; Lidor, G.; Vaxman, A.; Zuri, L. J Electrost, 1999, 47, 201.
6. Nagata, K.; Iwabuki, H.; Nigo, H. Compos Interfaces 1999, 6, 483.
7. Demain, A. Thermal Conductivity of Polymer-Chopped Carbon Fibre Composites, Ph.D. Dissertation, Universite Catholique de Louvain, Louvain-la-Neuve, Belgium, 1994.
8. King, J. A.; Tucker, K. W.; Meyers, J. D.; Weber, E. H.; Clingerman, M. L.; Ambrosius, K. R. Polym Compos 2001, 22, 142.
9. Murthy, M. V. Proceedings of the Society of Plastics Engineers Annu Technical Conference, 1994, p 1396.
10. Simon, R. M. Polym News 1985, 11, 102.
11. Mapleston, P. Mod Plast 1992, 69, 80.
12. Donnet, J.-B.; Bansal, R. C.; Wang, M.-J. Carbon Black, 2nd ed.; Marcel Dekker: New York, 1993.
13. Huang, J.-C. Adv Polym Technol 2002, 21, 299.
14. Bigg, D. M. Polym Compos 1987, 8, 1.
15. Hornbostel, B.; Potschke, P.; Koz, J.; Roth, S. Phys Stat Sol b 2006, 243, 3445.

16. Villmow, T.; Pegel, S.; Totschke, P.; Wagenknecht, U. Compos Sci Technol 2008, 68, 777.
17. Alig, I.; Skipa, T.; Lellinger, D.; Potschke, P. Polymer 2008, 49, 3524.
18. Shaffer, M. S. P.; Windle, A. H. Adv Mater 1999, 11, 937.
19. Chen, L.; Pang, X.-J.; Yu, Z.-L. Mater Sci Eng 2007, 457, 287.
20. Coleman, J. N.; Khan, U.; Gun'ko, Y. K. Adv Mater 2006, 18, 689.
21. Lopez Manchado, M. A.; Valentini, L.; Biagiotti, J.; Kenny, J. M. Carbon, 2005, 43, 1499.
22. Potschke, P.; Bhattacharyya, A. R.; Janke, A.; Goering, H. Compos Interf 2003, 10, 389.
23. Potschke, P.; Bhattacharyya, A.; Janke, A. Eur Polym J 2004, 40, 137.
24. Sandler, J.; Shaffer, M. S. P.; Prasse, T.; Bauhofer, W.; Schulte, K.; Windle, A. H. Polymer 1999, 40, 5967.
25. Potschke, P.; Bhattacharyya, A. R.; Janke, A. Carbon 2004, 42, 965.
26. Pegel, S.; Potschke, P.; Petzold, G.; Alig, I.; Dudkin, S. M.; Lellinger, D. Polymer 2008, 49, 974.
27. King, J. A.; Via, M. D.; Keith, J. M.; Morrison, F. A. J Comp Mater 2009, 43, 3073.
28. King, J. A.; Via, M. D.; Caspary, J. A.; Jubinski, M. M.; Miskioglu, I.; Mills, O. P.; Bogucki, G. R. J Appl Polym Sci 2010, 118, 2512.
29. Zhou, Z.; Wang, S.; Zhang, Y.; Zhang, Y. J Appl Polym Sci 2006, 102, 4823.
30. Zhang, Q.-H.; Chen, D.-J. J Mater Sci 2004, 39, 1751.
31. Feng, J.; Li, J.; Chan, C.-M. J Appl Polym Sci 2002, 85, 358.
32. Sabic Innovative Plastics PC Resin Product Brochure; Sabic-PLA-650, One Plastics Avenue: Pittsfield, MA, 2008.
33. Edwards, S. A.; Choudhury, N. R. Polym Eng Sci 2004, 44, 96.
34. Hyperion Catalysis International Fibril Product Literature; Hyperion Catalysis International, 38 Smith Place: Cambridge, MA, 2008.
35. Akzo Nobel Electrically Conductive Ketjenblack Product Literature; 300. S. Riverside Plaza: Chicago, IL, 1999.
36. Determination of Dynamic Mechanical Properties—Part 10: Complex Shear Viscosity Using a Parallel Plate Oscillatory Rheometer, ISO 6721-10:1999; International Standard Organization: Switzerland, 1999.
37. Morrison, F. A. Understanding Rheology; Oxford University Press: New York, 2001.
38. Cox, W. P.; Merz, E. H. J Polym Sci 1958, 28, 619.
39. Standard Test Methods for Determination of Properties of Polymeric Materials by Means of a Capillary Rheometer, ASTM Standard D3835-02; American Society for Testing and Materials: Philadelphia, 2002.
40. Standard Test Methods for DC Resistance or Conductance of Insulating Materials, ASTM Standard D257-91; American Society for Testing and Materials: Philadelphia, PA, 1998.
41. Standard Test Methods for DC Resistance or Conductance of Moderately Conductive Materials, ASTM Standard D4496-04; American Society for Testing and Materials: Philadelphia, PA, 2008.
42. King, J. A.; Morrison, F. A.; Keith, J. M.; Miller, M. G.; Smith, R. C.; Cruz, M.; Neuhalfen, A. M.; Barton, R. L. J Appl Polym Sci 2006, 101, 2680.
43. King, J. A.; Tambling, T. M.; Morrison, F. A.; Keith, J. M.; Cole, A. J.; Pagel, R. M. J Appl Polym Sci 2008, 108, 1646.
44. Kunen, E.; Keith, J. M.; Grant, P. W.; King, J. A.; Morrison, F. A. J Appl Polym Sci 2007, 106, 433.
45. King, J. A.; Tambling, T. M.; Keith, J. M.; Cole, A. J.; Morrison, F. A. Polym Compos 2009, 30, 111.
46. Shenoy, A. V. Rheology of Filled Polymer Systems; Klewer Academic Publishers: Boston, 1999.
47. Lee, S. H.; Kim, J. H.; Choi, S. H.; Kim, S. Y.; Kim, K. W.; Youn, J. R. Polym Int 2009, 58, 354.
48. Bird, R. B.; Armstrong, R. C.; Hassager, O. Dynamics of Polymeric Liquids; Wiley: New York, 1987.
49. King, J. A.; Via, M. D.; King, M. E.; Miskioglu, I.; Bogucki, G.R. J Appl Polym Sci (in press).